ELSEVIER

Nuclear Physics A 699 (2002) 963–975

NUCLEAR PHYSICS A

www.elsevier.com/locate/npe

Microscopic study of the ^{6}Li(p, γ)^{7}Be and ^{6}Li(p, α)^{3}He reactions

K. Arai, D. Baye, P. Descouvemont *

Physique Nucléaire Théorique et Physique Mathématique, CP 229, Université Libre de Bruxelles, B1050 Brussels, Belgium

Received 11 July 2001; revised 28 August 2001; accepted 7 September 2001

Abstract

A four-cluster microscopic model is used to investigate low-energy ^{6}Li + p and ^{6}Li + n reactions, as well as related reactions, of astrophysical interest. The model involves $\alpha + {}^3$He, ^{6}Li($1^+, 0^+$) + p and ^{6}Be(0^+) + n (or mirror) configurations with ^{3}He, ^{6}Li and ^{6}Be wave functions calculated variationally in a three-cluster description. The sensitivity to the model space of the ^{3}He(α, γ)^{7}Be and ^{3}H(α, γ)^{7}Li cross sections is discussed. The ^{6}Li(p, γ)^{7}Be cross section nicely agrees with experiment but some overestimation is obtained for ^{6}Li(p, α)^{3}He. The ^{6}Li(n, γ)^{7}Li and ^{6}Li(n, α)t reactions are also analyzed within the same model.

1. Introduction

Within recent years, a strong interest has been taken in low-energy reactions producing ^{7}Be and ^{7}Li in stellar environments [1,2]. Experiments and calculations concerning the ^{3}He(α, γ)^{7}Be and ^{3}H(α, γ)^{7}Li reactions are very numerous (see references in Refs. [1–3]). The former reaction is involved in the solar neutrino problems since it produces ^{7}Be which is destroyed through the ^{7}Be(p, γ)^{8}B process. The latter plays an important role in the big-bang nucleosynthesis.

The situation concerning the ^{6}Li(p, γ)^{7}Be and ^{6}Li(p, α)^{3}He reactions is different. The former has been experimentally studied by Switkowski et al. [4] at energies down to 200 keV. A theoretical extrapolation has been performed by Barker [5] within the potential model, based on a simultaneous fit of the ^{6}Li(n, γ)^{7}Li and ^{6}Li(p, γ)^{7}Be cross sections. The ^{6}Li(p, α)^{3}He cross section has been measured by several groups (see references in Ref. [2]); the latest experiment by Engstler et al. [6] aimed at analyzing electron screening effects at very low energies. To our knowledge, there is no theoretical study of this reaction.

* Directeur de Recherches FNRS. Corresponding author.
E-mail address: pdesc@ulb.ac.be (P. Descouvemont).

0375-9474/02/$ – see front matter
PII: S0375-9474(01)01298-2

In the present paper, we use a microscopic multicluster description of $A = 7$ systems. This model has been recently applied to low-energy ^{6}He + p reactions [7]. It involves ^{6}He + p, ^{6}Li$(1^+, 0^+)$ + n and α + t configurations where the ^{6}He, ^{6}Li and t wave functions are defined in a three-cluster approach. This description was shown in Ref. [7] to provide a fairly good description of the different thresholds and of ^{7}Li low-energy states. The same basis functions (or mirror) are used here to investigate several reactions. Within a common framework, we study the ^{3}He$(\alpha, \gamma)^7$Be, ^{6}Li$(\mathrm{p}, \gamma)^7$Be and ^{6}Li$(\mathrm{p}, \alpha)^3$He reactions. Elastic scattering and mirror reactions are also analyzed.

In Section 2, we give some information about the multicluster approach and about the calculation of transfer and capture cross sections. Section 3 is devoted to the spectroscopy of ^{7}Be and ^{7}Li, and to the different cross sections. Concluding remarks are presented in Section 4.

2. The model

We briefly present here the microscopic model and refer the reader to Ref. [7] for further detail. In a microscopic model, the Hamiltonian is given as

$$H = \sum_{i=1}^{A} T_i + \sum_{i<j=1}^{A} V_{ij}, \tag{1}$$

where A is the nucleon number, T_i is the kinetic energy of nucleon i and V_{ij} is an effective nucleon–nucleon interaction, involving nuclear and Coulomb components. We use the Minnesota force [8] (referred to as MN) as central part with the Reichstein–Tang spin–orbit interaction (set number IV) [9]. No well-established effective tensor force, adapted to the harmonic-oscillator cluster model, is available for the moment. The Minnesota interaction has been adjusted to the nucleon–nucleon scattering lengths, and simulates the role of the tensor force by increasing the triplet S interaction to fit the deuteron binding energy.

The 7-nucleon wave functions are defined in the Resonating Group Method (RGM), based on the assumption that two neutrons and two protons form an α cluster. In ^{7}Be, the first open channel is $\alpha + {}^3$He which is the natural cluster description of this nucleus. Since we want to investigate the ^{6}Li$(\mathrm{p}, \alpha)^3$He cross section, the ^{6}Li(1^+) + p channel must also be included. The basis is complemented by the ^{6}Li(0^+) + p and ^{6}Be(0^+) + n configurations. Although the ^{6}Be ground state is unstable against particle decay, the ^{6}Be(0^+) + n channel must be included in the basis to avoid unphysical isospin mixings. Schematically, the total wave function reads

$$\Psi^{JM\pi} = \Psi^{JM\pi}_{\alpha+{}^3\mathrm{He}} + \sum_{I_1=1^+,0^+} \Psi^{JM\pi}_{{}^6\mathrm{Li}(I_1)+\mathrm{p}} + \Psi^{JM\pi}_{{}^6\mathrm{Be}(0^+)+\mathrm{n}}, \tag{2}$$

where each component is given by

$$\Psi^{JM\pi}_{1+2} = \sum_{\ell I} \mathcal{A}\big[[\phi_1 \otimes \phi_2]^I \otimes Y_\ell(\hat{\boldsymbol{\rho}}_{12})\big]^{JM} \chi^{J\pi}_{1+2,\ell I}(\rho_{12}). \tag{3}$$

In this equation, I is the channel spin, $\mathcal{A}$ is the A-nucleon antisymmetrizer which accounts for the Pauli principle, and $\boldsymbol{\rho}_{12}$ the relative coordinate between fragments 1 and 2. The internal wave functions ϕ_1 and ϕ_2 are themselves defined in the multicluster model. The ^{6}Li and ^{6}Be wave functions are expanded over a set of $\alpha + \mathrm{p} + \mathrm{n}$ and $\alpha + \mathrm{p} + \mathrm{p}$ configurations, respectively; the ^{3}He wave function is defined in a $\mathrm{p} + \mathrm{p} + \mathrm{n}$ model. As shown in Ref. [7], this multicluster approach provides fairly good properties for these nuclei. The halo structure of ^{6}He and $^6\mathrm{Li}(0^+)$ is well reproduced, and the theoretical breakup thresholds in ^{7}Be and ^{7}Li are in good agreement with experiment. Our multicluster model is similar to that of Mertelmeier and Hofmann [10] who do not consider the $^6\mathrm{Li}(0^+) + \mathrm{p}$ and $^6\mathrm{Be}(0^+) + \mathrm{n}$ configurations. The same difference holds for the recent work [3] of Csótó and Langanke who approximate the ^{6}Li wave function as a two-cluster $\alpha + \mathrm{d}$ structure. Those works only focus on the $^3\mathrm{He}(\alpha,\gamma)^7\mathrm{Be}$ and mirror reactions.

The unknown quantities in Eq. (3) are the relative functions $\chi^{J\pi}_{1+2,\ell I}(\rho_{12})$. They are expanded over a set of Gaussian functions centered at $\rho_{12} = 0$ and characterized by different width parameters (15 in the present case [7]). This expansion enables one to compute matrix elements in an analytical way [7] and avoids the numerical integration occurring in multicluster models with expansion over shifted Gaussian functions [11]. The correct asymptotic treatment of the wave functions is achieved through the use of the microscopic R-matrix method [12,13] for bound as well as for scattering states.

The transfer cross section from an initial channel i to a final channel f is given by

$$\sigma_{if}(E) = \frac{\pi}{k^2} \sum_{J\pi} \frac{2J+1}{(2I_1+1)(2I_2+1)} \sum_{\ell_i \ell_f I_i I_f} \left| U^{J\pi}_{i\ell_i I_i, f\ell_f I_f}(E) \right|^2, \tag{4}$$

where E is the cm energy, k is the wave number, I_1 and I_2 are the spins of the colliding nuclei, in the entrance channel, and $U^{J\pi}(E)$ is the collision matrix. On the other hand, the capture cross section to a final bound state with wave function $\Psi^{J_f\pi_f}$ reads

$$\begin{aligned} \sigma_\gamma(E, J_f\pi_f) = {} & \frac{2J_f+1}{(2I_1+1)(2I_2+1)} \frac{8\pi}{\hbar} \left(\frac{E_\gamma}{\hbar c}\right)^{2\lambda+1} \frac{(\lambda+1)}{\lambda(2\lambda+1)!!^2} \\ & \times \sum_{J_i I_i \ell_i} \frac{1}{(2\ell_i+1)} \left| \left\langle \Psi^{J_f\pi_f} \middle|\middle| \mathcal{M}^E_\lambda \middle|\middle| \Psi^{J_i\pi_i}_{\ell_i I_i}(E) \right\rangle \right|^2, \end{aligned} \tag{5}$$

where $\mathcal{M}^E_\lambda$ represents the electric multipole operator of rank λ (we only consider the E1 multipolarity here) and E_γ is the photon energy. The initial wave function is assumed to be a partial wave of a unit-flux scattering wave function [14].

3. Results

3.1. Spectroscopy of ^{7}Li and ^{7}Be

Let us first study the low-energy spectrum of ^{7}Be. In Fig. 1, we present the energies of the $3/2^-$, $1/2^-$, $7/2^-$ and $5/2^-$ states and the $^6\mathrm{Li}(1^+, 0^+) + \mathrm{p}$ thresholds. These states are known to be the members of a rotational band and are important for the reactions studied

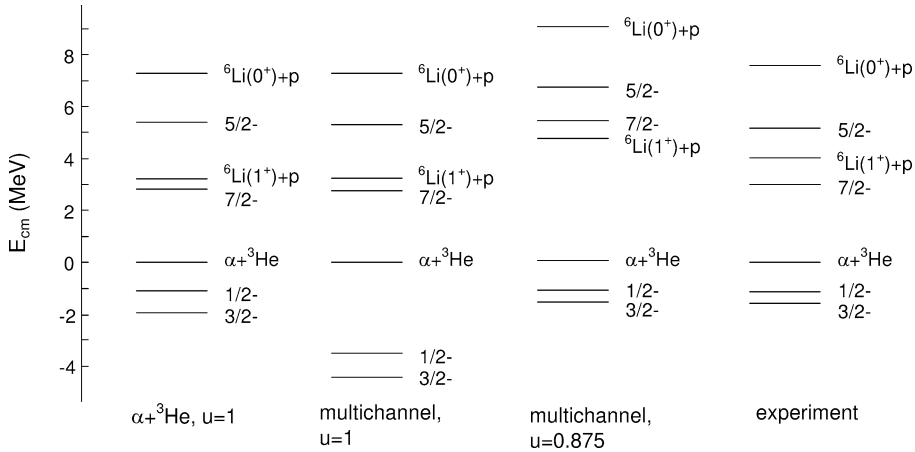

Fig. 1. ^{7}Be spectra with different conditions of calculation: single-channel and multichannel (see text). Experimental data are taken from Ref. [15].

here. The model predicts other states, but they are not in the energy range relevant for the reactions considered here. We refer to Ref. [7] for their energies. Energies are given with respect to the $\alpha + {}^{3}$He threshold. First we perform a single-channel $\alpha + {}^{3}$He calculation with the standard value of the exchange parameter $u = 1$. This yields a ^{7}Be ground state overbound by 0.4 MeV, but the $1/2^-$ excited state and the narrow $7/2^-$ resonance are located very close to the experimental values. For the broad $5/2^-$ resonance ($\Gamma_\alpha \simeq 1$ MeV), the width does not enable a precise determination of the energy. The same interaction provides $^{6}\mathrm{Li}(1^+) + \mathrm{p}$ and $^{6}\mathrm{Li}(0^+) + \mathrm{p}$ thresholds in good agreement with experiment.

Using the same interaction with the full basis weakly affects the $7/2^-$ and $5/2^-$ resonances, but increases the binding energy of the $3/2^-$ and $1/2^-$ states by about 2.5 MeV. This result was already found out in Ref. [7] and is due to some limitations of the MN force for multichannel calculations. It has been optimized on $\alpha + \alpha$ scattering with distortion of the α particles [8]. The present calculation with the $\alpha + {}^{3}$He channel only is similar to those conditions and, consequently, makes the MN force well adapted. However, mixing with other cluster structures has not been explicitly considered in the MN interaction and the coupling between $\alpha + {}^{3}$He and $^{6}\mathrm{Li} + \mathrm{n}$ configurations is most likely overestimated.

This effect has been compensated by readjusting the exchange parameter to $u = 0.875$ which provides the experimental ground-state energy. This requirement is crucial to obtain realistic capture cross sections. The other energies ($7/2^-$, $5/2^-$ and $^{6}\mathrm{Li}(1^+, 0^+) + \mathrm{p}$ thresholds) are not too severely modified. The value $u = 0.875$ has been used for all multichannel calculations. With this interaction, states other than those presented in Fig. 1 are in the continuum. These resonances are very broad and realistic values for their energies and widths can not be determined.

In Table 1, we give spectroscopic properties of ^{7}Be. We also present the quadrupole moment and $B(\mathrm{E2})$ value in the mirror nucleus ^{7}Li. The α and p dimensionless reduced widths are calculated at 6 fm. The α reduced widths represent about 10% of the Wigner

Table 1
Spectroscopic properties of ^{7}Be and ^{7}Li

^{7}Be	Single channel	Multichannel	Exp. [15]
$\theta^2_\alpha(3/2^-)$	0.10	0.12	
$\theta^2_\alpha(1/2^-)$	0.13	0.12	
$\theta^2_\alpha(5/2^-)$	~ 0.25	~ 0.35	0.31
$\theta^2_\alpha(7/2^-)$	~ 0.26	~ 0.22	0.12 ± 0.01
$\theta^2_p(3/2^-)$	–	0.024	
$\theta^2_p(1/2^-)$	–	0.031	
$Q(3/2^-)$	-5.6	-6.4	
$B(\mathrm{E2}, 1/2^- \to 3/2^-)$	36.9	44.7	
^{7}Li			
$Q(3/2^-)$	-3.42	-3.57	-4.06 ± 0.08
$B(\mathrm{E2}, 1/2^- \to 3/2^-)$	13.0	13.1	16.6 ± 1.0

The dimensionless reduced widths are calculated at 6 fm. The quadrupole moments are expressed in e fm^2 and the B(E2) values in e^2 fm^4.

limit, which confirms the cluster structure of the ^{7}Be low-lying states. These values are weakly sensitive to the number of channels. In the multichannel calculation, the proton reduced widths are 2% and 3% for the $3/2^-$ and $1/2^-$ states, respectively. These numbers are not negligible, and confirm the conclusion drawn from Fig. 1, i.e. that the proton channels affect the ^{7}Be ground and first excited states. With the potential of Ref. [5] fitted to the theoretical energies, we obtain the spectroscopic factors $C^2S = 0.72$ $(3/2^-)$ and 0.84 $(1/2^-)$ for the ^{6}Li(1^+) + p configuration. The ground-state value is known experimentally ($C^2S = 0.87$—see Ref. [15]) for the mirror nucleus ^{7}Li, and is slightly larger than the present calculation. The $7/2^-$ and $5/2^-$ resonances are rather broad and have a dominant $\alpha + {}^3$He structure. Their proton widths can not be determined with accuracy and are consistent with zero.

In ^{7}Li, the quadrupole moment and the B(E2) value do not significantly depend on the proton channels. This was also found out by Csótó and Langanke [3] who find similar values. The model slightly underestimates the quadrupole moment and the B(E2) value.

In ^{7}Be, the sensitivity to the number of channels is larger. Including ^{6}Li + p configurations introduces polarization effects and therefore modifies the deformation of ^{7}Be. Experimental values would be welcome to test the models.

3.2. *The ^{3}He$(\alpha,\gamma)^7$Be and ^{3}H$(\alpha,\gamma)^7$Li reactions*

Before showing the capture cross sections, let us first discuss the $\alpha + {}^3$He elastic phase shifts presented in Fig. 2. The $3/2^+$ phase shift ($\ell = 2$) is very small in the considered energy range. The $1/2^+$ phase shift ($\ell = 0$) is characteristic of a hard-sphere behaviour. As observed in Ref. [3], the effect of ^{6}Li + p configurations is rather weak, and of the same amplitude as the uncertainty due to the nucleon–nucleon interaction [3]. The $5/2^+$ phase

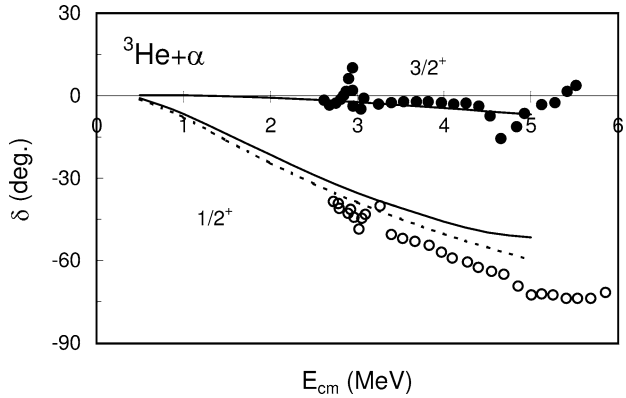

Fig. 2. $\alpha + {}^3\mathrm{He}$ elastic phase shifts in the multichannel (full curves) and single-channel (dotted curves) models. For $J = 3/2^+$ the curves are indistinguishable. The data are taken from Ref. [16].

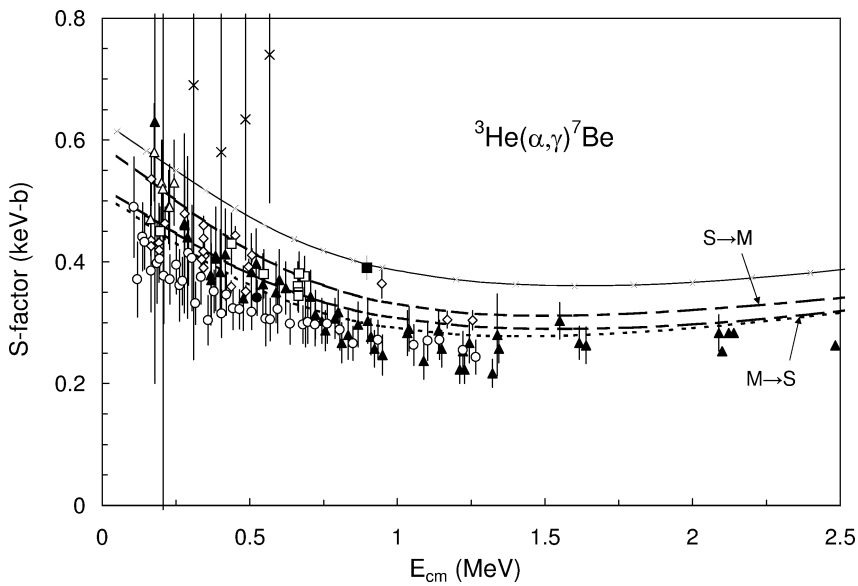

Fig. 3. ${}^3\mathrm{He}(\alpha,\gamma){}^7\mathrm{Be}$ S-factor for different conditions of calculation: multichannel (full curve), single channel (dotted curve), and single channel for the initial state and multichannel for the final state (S → M). The reverse conditions are labeled by M → S. The symbols follow the notations of Ref. [2].

shifts are very similar to the $3/2^+$ data [16]; negative-parity phase shifts do not affect the capture cross section and are therefore not shown here.

The ${}^3\mathrm{He}(\alpha,\gamma){}^7\mathrm{Be}$ S-factor is given in Fig. 3. We first perform a single-channel calculation with the ${}^3\mathrm{He} + \alpha$ channel only. The u parameter has been slightly modified for both the $3/2^-$ and $1/2^-$ states in order to reproduce their experimental energies. The theoretical S-factor gives a good fit of the data, although the experimental uncertainties are large. At zero energy, we have $S(0) = 0.52$ keV b and $s_1 = S(0)^{-1}(\mathrm{d}S/\mathrm{d}E)_0 = -0.63$ MeV^{-1}. The present S-factor is in very good agreement with the calculations

of Mertelmeier and Hofmann [10] and of Kajino [17]. Csótó and Langanke [3] find a normalization 20% larger ($S(0) = 0.70$ MeV b) although they use the same MN interaction, but with different parameters. This confirms the sensitivity of the S-factor with respect to the model description [3].

As mentioned in previous studies [3,10], introducing ^{6}Li + p configurations provides an overestimation of the data ($S(0) = 0.63$ keV b, $s_1 = -0.57$ MeV^{-1}). This problem is related to the discussion of Section 3.1 concerning the ability of the MN force to describe multichannel calculations. The multichannel approach yields a larger deformation (see Table 1) which in turn is responsible for an enhancement of the S-factor.

In order to understand the role of the ^{6}Li + p distortion channel, we have performed two complementary calculations. In the first one (M → S), we have used the single-channel approximation for the bound state only. This result is very similar to the S-factor obtained in the single-channel model; it is consistent with a dominant extranuclear capture. On the other hand, using a single-channel approximation for the initial scattering state (S → M) is more different from the single-channel calculation. The reason is that contributions coming from ^{6}Li + p configurations are not external, and that the S-factor is not simply proportional to the amplitude of the final wave function. Notice that the slope of the S-factor at low energies is also sensitive to the model.

The ^{3}H$(\alpha,\gamma)^7$Li S-factor is given in Fig. 4. The conclusions are quite similar to those of ^{3}He$(\alpha,\gamma)^7$Be. The single-channel calculation nicely reproduces the data, whereas introducing ^{6}Li + n configurations provides too large an S-factor.

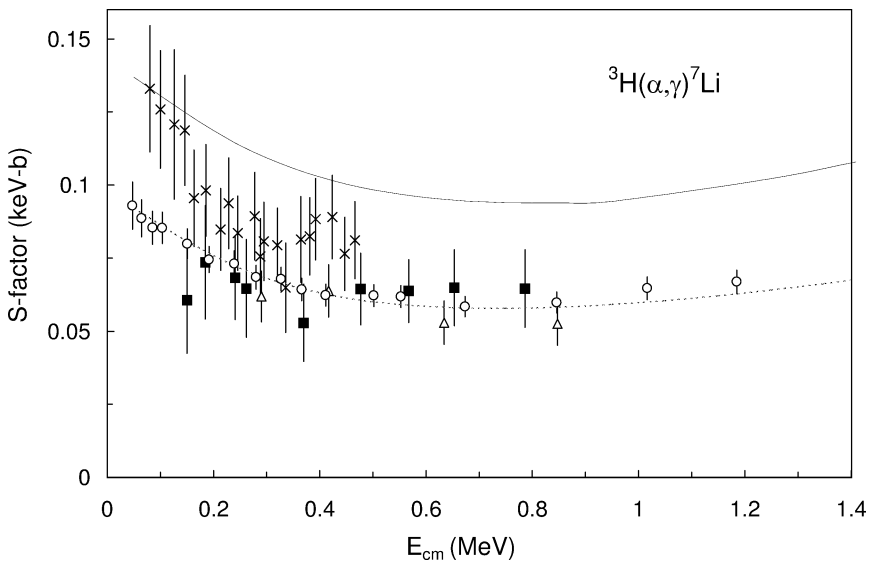

Fig. 4. ^{3}H$(\alpha,\gamma)^7$Li S-factor for different conditions of calculation: multichannel (full curve) and single channel (dotted curve). The symbols follow the notations of Ref. [2].

3.3. $^6Li + n$ elastic scattering and reactions

The low-energy s-wave phase shifts can be parameterized in the scattering-length formalism. The real part of the scattering length a_I is defined as

$$a_I = -\lim_{k\to 0} \frac{\tan\delta_I(k)}{k}, \tag{6}$$

where $\delta_I(k)$ is the s phase shift in partial wave $I = 1/2$ or $3/2$. The experimental values [15] are

$$a_{1/2} = 4.67 \pm 0.17 \text{ fm}, \qquad a_{3/2} = 0.67 \pm 0.14 \text{ fm}. \tag{7}$$

These data show that the $1/2^+$ partial wave is strongly dominant. The present model provides

$$a_{1/2} = 4.1 \text{ fm}, \qquad a_{3/2} = 2.3 \text{ fm}. \tag{8}$$

For $I = 1/2$, the theoretical result is in reasonable agreement with experiment, but the RGM value for $I = 3/2$ enhances the low-energy phase shift by a factor of 3.

The ^{6}Li(n, α)t cross section is presented in Fig. 5. As explained in Section 2, the energy of the $5/2^-$ resonance is higher in our model than observed experimentally. Consequently this resonance does not show up in the energy range considered in Fig. 5. The present cross section is in good agreement with the nonresonant part of the data. At thermal energy, we have, from experiment [15]

$$\sigma_{n\alpha} = 940 \pm 4 \text{ b}, \tag{9}$$

which is well reproduced by the calculation

$$\sigma_{n\alpha} = 892 \text{ b}. \tag{10}$$

The thermal cross section can be decomposed as

$$\sigma_{n\alpha} = \frac{1}{3}\sigma_{n\alpha}(1/2) + \frac{2}{3}\sigma_{n\alpha}(3/2), \tag{11}$$

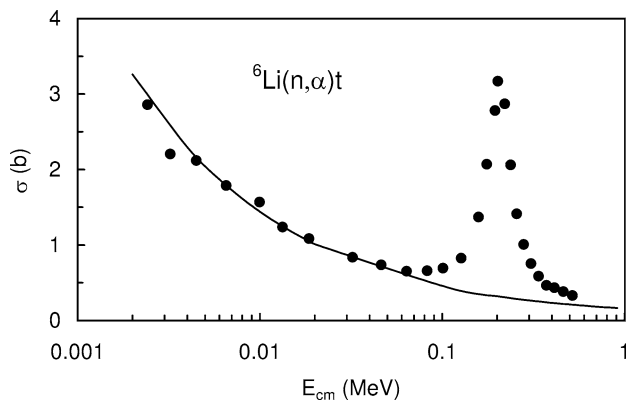

Fig. 5. ^{6}Li(n, α)t cross section. The data are taken from Ref. [19].

which involves the partial cross sections corresponding to $I = 1/2$ and $I = 3/2$. Experimentally, the branching ratio [18] is

$$\frac{\sigma_{n\alpha}(3/2)}{\sigma_{n\alpha}(1/2)} = 0.127 \pm 0.016. \tag{12}$$

This value is strongly underestimated by the calculation (7.0×10^{-6}). Qualitatively, the model is consistent with a dominance of the $1/2$ partial wave, and its contribution is well explained. The ^{6}Li(n, α)t reaction involves $\ell_i = 0 \to \ell_f = 0$ and $\ell_i = 0 \to \ell_f = 2$ transitions in the $1/2^+$ and $3/2^+$ partial waves, respectively. An accurate treatment of the $3/2^+$ contribution therefore requires a tensor component in the nucleon–nucleon interaction, which is missing here. The central and spin–orbit terms provide a very weak coupling through the other channels, but can not account for the experimental value. This coupling problem is responsible for the overestimation of the $a_{3/2}$ scattering length, mentioned above, and leads to a very poor description of the transfer branching ratio.

Let us now come to the ^{6}Li(n, γ)^{7}Li cross section. It is presented in Fig. 6 as the reverse photodissociation cross section from the Q value $E_\gamma = 7.25$ MeV to 9 MeV. Only the dominant E1 multipolarity is included in the multipole expansion. Consequently, the $5/2^-$ resonance which appears as a broad bump in the data near $E_\gamma = 7.5$ MeV does not show up in the RGM cross section since it would require M1 or E2 multipolarities.

At thermal energy, the capture cross section $\sigma_{n\gamma}$ and the ground-state branching ratio $\mathcal{R}$ are experimentally known as

$$\sigma_{n\gamma} = 38.5 \pm 3.0 \text{ mb}, \qquad \mathcal{R} = 0.62 \pm 0.02, \tag{13}$$

and the corresponding RGM results

$$\sigma_{n\gamma} = 28.9 \text{ mb}, \qquad \mathcal{R} = 0.65, \tag{14}$$

agree reasonably well with the data.

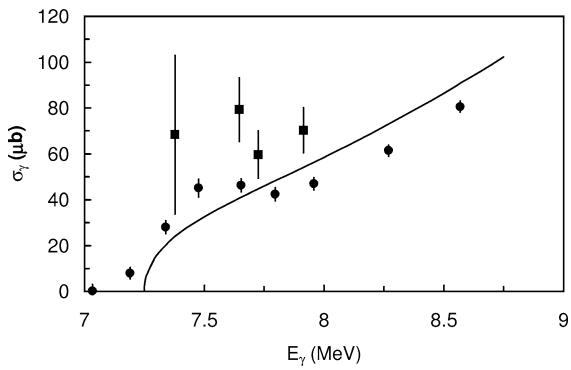

Fig. 6. ^{7}Li photodissociation cross section. The data are taken from Ref. [20] (circles, with energies increased by 0.1 MeV, as suggested in Ref. [5]) and Ref. [21] (squares).

3.4. $^6Li + p$ elastic scattering and reactions

The s-wave elastic phase shifts are presented in Fig. 7. Up to 2 MeV the $1/2^+$ data [22] are well reproduced by the model. The repulsive behaviour of the $3/2^+$ phase shift is also present in the RGM but the energy dependence is too steep.

The ^{6}Li(p, α)^{3}He reaction plays a role in stellar evolution since it produces ^{3}He which is converted in α particles through the ^{3}He(^{3}He, 2p)^{4}He reaction. The ^{6}Li(p, α)^{3}He cross section has been measured by many groups (see references in Ref. [2]). The latest measurement [6] was aimed at investigating electron screening effects in this reaction with data obtained at very low energies ($E_{cm} \approx 0.01$ MeV). These data, shown in Fig. 8, were fitted by Engstler et al. [6] with a polynomial expansion of the S-factor at energies larger than 0.1 MeV. Extrapolation of this fit down to zero energy provides an estimate of the screening potential.

The RGM results, presented in Fig. 8 (full curve), are obtained without any parameter fit, and do not include any screening effects. Fig. 8 shows that the order of magnitude of the experimental data is well reproduced but the shape of the cross section is apparently in

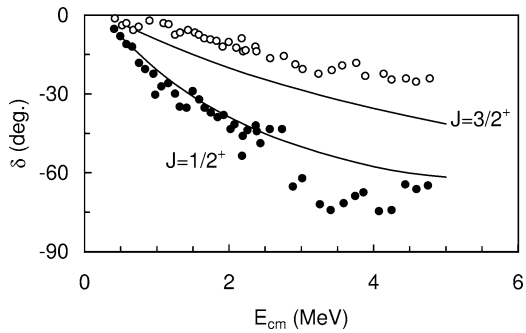

Fig. 7. ^{6}Li + p elastic phase shifts. The data are taken from Ref. [22].

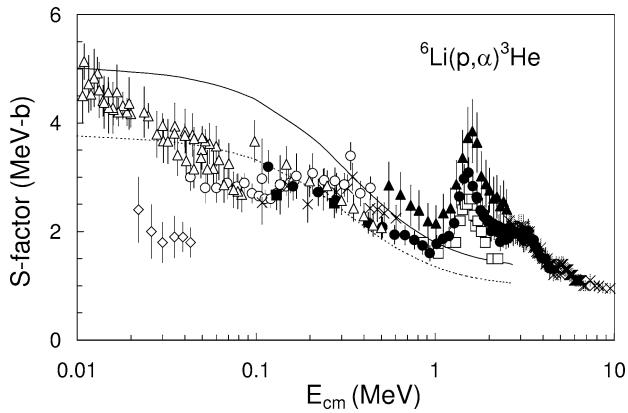

Fig. 8. ^{6}Li(p, α)^{3}He S-factors without (full curve) and with (dotted curve) a renormalization factor 0.75 (see text). The symbols follow the notations of Ref. [2].

disagreement with experiment. Most likely the RGM overpredicts the data. This effect has been met in the similar ^{7}Li(p, α)^{4}He reaction [11], where a multicluster RGM calculation also overestimates the experimental data. The origin of this problem arises from the fact that a cluster description of ^{6}Li (or ^{7}Li) assumes that the α wave function is identical to the wave function of a free α particle. This simplifying assumption is necessary in the present model, but overestimates the overlap between the $\alpha + {}^3$He and ^{6}Li + p channels. To illustrate this property, we have renormalized the RGM S-factor by 0.75 (dotted curve in Fig. 8). This factor simulates an overlap reduction, and provides a good agreement with the data between 0.1 and 1 MeV. Below 0.1 MeV, the data are affected by electron screening effects and are consequently larger than the present scaled results. Let us mention that the main contribution to the S-factor is given by the $1/2^+$ partial wave ($\ell = 0$). As for ^{6}Li(n, α)t, the $3/2^+$ contribution involves a $\ell_i = 0 \to \ell_f = 2$ transition which would require a tensor force. Notice that the RGM contribution of the $5/2^-$ partial wave is lower than contributions of the other partial waves. The peak observed in the data near 1.6 MeV, due to a $5/2^-$ resonance, is therefore not present in the theoretical cross section.

The ^{6}Li(p, γ)^{7}Be reaction has been studied experimentally by Switkowski et al. [4] from 0.2 to 1 MeV. Data corresponding to the $1/2^-$ excited state [24] and preliminary data from the Athens group [25] are also available. A calculation by Barker [5] within the potential model aims at analyzing the ^{6}Li + n and ^{6}Li + p mirror systems simultaneously. The RGM capture cross section is displayed in Fig. 9 where only the E1 multipolarity has been introduced. In the calculation of the photon energy, experimental values for the ^{7}Be $3/2^-$ and $1/2^-$ energies have been used in order to correct for slight inaccuracies of the model energies (see Fig. 1). Without any spectroscopic factor, the theoretical S-factor is consistent with the data, although slightly lower. At zero energy, we have

$$S(0) = 105 \text{ eV b}. \tag{15}$$

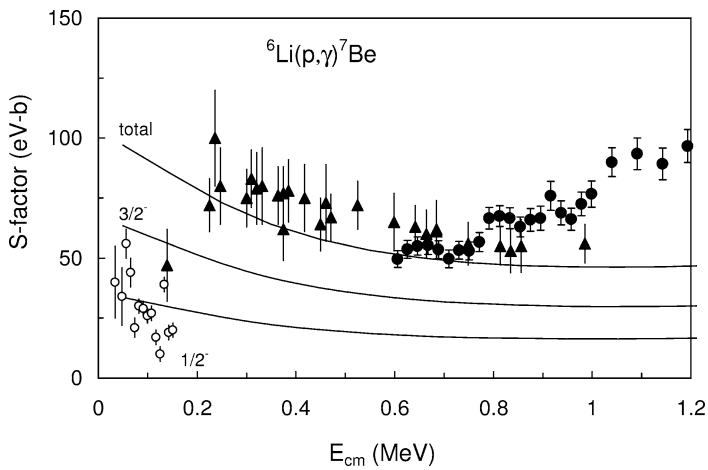

Fig. 9. ^{6}Li(p, γ)^{7}Be S-factor with the partial contributions of the ^{7}Be final states. The data are from Ref. [4] (triangles), Ref. [25] (filled circles), and Ref. [24] (open circles—$1/2^-$ contribution).

This result confirms that the ^{6}Li(p, γ)^{7}Be reaction rate should be larger than recommended in Ref. [23], as it was pointed out by the NACRE collaboration [2]. The partial S-factor corresponding to capture to the $1/2^-$ excited state is in good agreement with the low-energy data of Ref. [24]. At zero energy the RGM branching ratio (35%) is consistent with experiment [4] ($39 \pm 2\%$).

4. Conclusions

We have studied several reactions involving ^{7}Be and ^{7}Li as unified nucleus. The model includes $\alpha + {}^3$He, ^{6}Li$(1^+, 0^+)$ + p and ^{6}Be(0^+) + n configurations (or mirror) with realistic cluster wave functions. It has been previously applied to reactions involving the ^{6}He halo nucleus [7]. Calculations of the ^{3}He$(\alpha, \gamma)^7$Be and ^{3}H$(\alpha, \gamma)^7$Li S-factors confirm [3,10] that including $6 + 1$ configurations makes the RGM less good than the single-channel approach. This problem is most likely due to the effective nucleon–nucleon interaction which simulates the tensor force in the central part, and which is fitted on single-channel results.

The present model provides a fairly good description of several ^{6}Li + p and ^{6}Li + n reactions. The ^{6}Li(p, γ)^{7}Be RGM S-factor is in good agreement with the available experimental data. For the ^{6}Li(p, α)^{3}He transfer reaction, a normalization factor is necessary to compensate the strong coupling between the $\alpha + {}^3$He and ^{6}Li + p configurations. Transfer reactions are known to be more sensitive to the cluster description than capture reactions. On the other hand, the ^{6}Li(n, γ)^{7}Li and ^{6}Li(n, α)t cross sections are well described by the model. The present results suggest that the $I = 3/2$ contribution in the ^{6}Li(n, α)t and ^{6}Li(p, α)^{3}He cross sections could be used to test a tensor component in the nucleon–nucleon interaction.

Acknowledgements

We are grateful to Th. Paradellis for providing us with preliminary data on the ^{6}Li(p, γ)^{7}Be S-factor. This paper presents research results of the Belgian Program P4/18 on interuniversity attraction poles initiated by the Belgian-state Federal Services for Scientific Technical and Cultural Affairs.

References

[1] E.G. Adelberger, S.M. Austin, J.N. Bahcall, A.B. Balantekin, G. Bogaert, L.S. Brown, L. Buchmann, F.E. Cecil, A.E. Champagne, L. de Braeckeleer, C.A. Duba, S.R. Elliott, S.J. Freedman, M. Gai, G. Goldring, C.R. Gould, A. Gruzinov, W.C. Haxton, K.M. Heeger, E. Henley, C.W. Johnson, M. Kamionkowski, R.W. Kavanagh, S.E. Koonin, K. Kubodera, K. Langanke, T. Motobayashi, V. Pandharipande, P. Parker, R.G.H. Robertson, C. Rolfs, R.F. Sawyer, N. Shaviv, T.D. Shoppa, K.A. Snover, E. Swanson, R.E. Tribble, S. Turck-Chièze, J.F. Wilkerson, Rev. Mod. Phys. 70 (1998) 1265.

[2] C. Angulo, M. Arnould, M. Rayet, P. Descouvemont, D. Baye, C. Leclercq-Willain, A. Coc, S. Barhoumi, P. Aguer, C. Rolfs, R. Kunz, J.W. Hammer, A. Mayer, T. Paradellis, S. Kossionides, C. Chronidou, K. Spyrou, S. Degl'Innocenti, G. Fiorentini, B. Ricci, S. Zavatarelli, C. Providencia, H. Wolters, J. Soares, C. Grama, J. Rahighi, A. Shotter, M. Lamehi Rachti, Nucl. Phys. A 656 (1999) 3.
[3] A. Csótó, K. Langanke, Few-Body Systems 29 (2000) 121.
[4] Z.E. Switkowski, J.C.P. Heggie, D.L. Kennedy, D.G. Sargood, F.C. Barker, R.H. Spear, Nucl. Phys. A 331 (1979) 50.
[5] F.C. Barker, Aust. J. Phys. 33 (1980) 159.
[6] S. Engstler, G. Raimann, C. Angulo, U. Greife, C. Rolfs, U. Schröder, E. Somorjai, B. Kirch, K. Langanke, Z. Phys. A 342 (1992) 471.
[7] K. Arai, P. Descouvemont, D. Baye, Phys. Rev. C 63 (2001) 044611.
[8] D.R. Thompson, M. LeMere, Y.C. Tang, Nucl. Phys. A 286 (1977) 53.
[9] I. Reichstein, Y.C. Tang, Nucl. Phys. A 158 (1970) 529.
[10] T. Mertelmeier, H.M. Hofmann, Nucl. Phys. A 459 (1986) 387.
[11] P. Descouvemont, D. Baye, Nucl. Phys. A 573 (1994) 28.
[12] D. Baye, P.-H. Heenen, M. Libert-Heinemann, Nucl. Phys. A 291 (1977) 230.
[13] K. Fujimura, D. Baye, P. Descouvemont, Y. Suzuki, K. Varga, Phys. Rev. C 59 (1999) 817.
[14] D. Baye, P. Descouvemont, Nucl. Phys. A 407 (1983) 77.
[15] F. Ajzenberg-Selove, Nucl. Phys. A 490 (1988) 1.
[16] R.J. Spiger, T.A. Tombrello, Phys. Rev. 163 (1967) 964.
[17] T. Kajino, Nucl. Phys. A 460 (1986) 559.
[18] H. Glättli, A. Abragam, G.L. Bacchella, M. Fourmond, P. Mériel, J. Piesvaux, M. Pinot, Phys. Rev. Lett. 40 (1978) 748.
[19] H.D. Knox, D.A. Resler, R.O. Lane, Nucl. Phys. A 466 (1987) 245.
[20] R.L. Bramblett, B.L. Berman, M.A. Kelly, J.T. Caldwell, S.C. Fultz, in: Proc. Int. Conf. on Photonuclear Reactions and Applications, Asilomar, 1973, Vol. 1, p. 175.
[21] L. Green, D.J. Donahue, Phys. Rev. 135 (1964) B701.
[22] C. Petitjean, L. Brown, R.G. Seyler, Nucl. Phys. A 129 (1969) 209.
[23] G.R. Caughlan, W.A. Fowler, At. Data Nucl. Data Tables 40 (1988) 283.
[24] R. Bruss, O. Arkis, H. Bucka, P. Heide, in: F. Käppeler, K. Wisshak (Eds.), Proc. Nuclei in the Cosmos, Karlsruhe, Germany, 1992, IOP, 1993, p. 169.
[25] T. Paradellis et al., private communication.